Front. Optoelectron. 2015, 8(3): 329–340
DOI 10.1007/s12200-015-0476-0

RESEARCH ARTICLE

Analysis and modeling of ridge waveguide quarterly wavelength shifted distributed feedback laser with three rate equations

Abbas GHADIMI (✉), Alireza AHADPOUR SHAL

Department of Electrical Engineering, Lahijan Branch, Islamic Azad University, Lahijan, Iran

Abstract In this paper, ridge waveguide quarterly wavelength shifted distributed feedback (RW-QWS-DFB) laser was modeled and analyzed. In this behavioral model, some characteristics of the device, such as threshold current, line width, power of output wave, spectrum of output wave, and laser stability in high powers, were investigated in accordance with different physical and geographical parameters such as sizes and structures of the layers. Considering a new proposed algorithm, the analysis of the mentioned structures was performed using transfer matrix method (TMM), the solution of coupled waves and carrier rate equations. The results showed the advantages of some parameters in this structure.

Keywords distributed feedback laser, transfer matrix method (TMM), transversal and lateral mode

1 Introduction

Invention of semiconductor lasers in 1960s and optical fibers in the early 1970s have resulted in ever-more-increasing improvement of global communications. Due to the higher external efficiency, the ability of direct modulation, and the small scalability of the semiconductor lasers, they are considered as convenient wave sources for optical communications. Conventional Fabry-Perot (FP) semiconductor lasers, are not single mode and do not fulfil the requirement of optical communication applications. Whereas, novel and advanced distributed feedback (DFB) semiconductor lasers, are widely used as wave sources in optical communication systems. Accordingly, nowadays, development of DFB lasers' design, qualities, and operation methods as well as their physical and numerical modeling has been the subjects of many researches.

The first semiconductor laser was constructed using a single crystal GaAs bipolar p-n junction [1–5]. Optical amplification in a semiconductor laser is similar to that in FP [6]. To reduce threshold current density in room temperature and modify semiconductor lasers' characteristics, single hetero (SH) structure was introduced in 1962 [7–9], and in late 1960s double-hetero (DH) structure was introduced to reduce threshold current down to 1 kA/cm^2 [10–12].

In many applications of semiconductor laser, the output waves enters an optical fiber, so that it is necessary for the light beam diameter to be smaller than optical fiber diameter, which is about a wavelength and much smaller than laser width. In this regard, stripe-geometry structure was employed to limit injected carrier flow and optical field in lateral direction [13].

Buried heterostructure (BH) was designed in 1975, and it can eliminate electrical current leakage in lateral direction and reduce threshold current [14]. In BH structures, active layer of the laser is surrounded in four directions by a material with lower refractive index (higher band gap). BH structure implementation is fairly difficult and complicated.

Another structure that was proposed and constructed to confine optical field, electrical current and electrical carriers was ridge-waveguide [15]. This structure has high modulation speed, while its threshold current is less than broad area structure and more than BH structure. Since the effective refractive index in lateral area and outside the ridge is less than middle area under the ridge, wave propagates (travels) under the ridge area.

Another proposed structure was rib-waveguide, which was identical to ridge-waveguide [16]. BH, ridge-waveguide, and rib-waveguide structures are generally called as index-guided structures. With modifications performed in

Received August 13, 2014; accepted October 16, 2014

E-mail: ghadimi@liau.ac.ir, a_ahadpour@liau.ac.ir

these structures of the semiconductor lasers, information transfer rate in optical fibers reached up to 140 Mbit/S in 1980 [17].

There have been successful approaches to increase the output power of the semiconductor lasers utilizing laser-array. In addition, providing some modification in structure of the arrays, this type of lasers has been employed in wavelength-division multiplexing (WDM) [18,19].

Vertical cavity surface emitting laser diode (VCSELD) is designed and developed for the applications, in which the light should be emitted in vertical direction to the junction [20].

Some other characteristics of semiconductor lasers, like line width, noise, and threshold current, have been modified using quantum well structures [21]. To make laser single mode, FP laser with external cavity has been proposed [22]. The great sensitivity of the structure to the changes of temperature and cavity length is a disadvantage of the structure. Using grating instead of external mirror in external cavity structure is another way to adjust wavelength and make semiconductor laser single mode. In this structure, line bandwidth can be reduced down to 100 kHz, and adjustability of wavelength is about several tens of nano-meters. But the installation of this compound system is very hard and it is so expensive for optical communication systems [23].

Apart from the above mentioned structures, cleaved coupled cavity (C^3) has been suggested to construct a single mode laser with adjustable wavelength. This was obtained by a very short distanced coupling (less than 1 μm) of the main laser with a shorter wavelength FP laser [24–26]. The best and most suitable method that has been used for construction of single mode semiconductor laser is creation of refractor grating inside the laser. DFB and distributed Bragg reflector (DBR) are two structures that were constructed base on this method. Investigations on DBR is started in early 1970s approximately at the same time with DFB lasers, but DBR lasers are more complicated with less applications [27].

The most common way to create grating is holographic technique and interaction of two coherent waves [28]. The first DFB lasers could work in low temperatures and had a short life time [29,30]. In the middle of 1970s, the first GaAs DFB laser was made that could work in room temperature [31]. In 1981 and 1982, the first DFB lasers with the wavelengths of 1.3 and 1.57 μm were constructed [32,33]. Construction of these two lasers has improved the fiber optic communication because the optical fibers have the lowest power consumption in these two wavelengths. Experimental and theoretical studies show that the DFB lasers with uniform grating and anti-reflective (AR) sides at endings oscillate in two symmetric (chirp) modes with respect to the Bragg frequency. Thus, conventional DFB laser is no single mode [28]. Several methods have been proposed to eliminate this degeneration, the most important ones are:

1) Cavity has nonzero reflective index at the two ending sides of the laser [34].

2) Creation of asymmetry (chirp) in the period of the grating [35].

3) Creation of a phase shift equal to $\lambda / 4$ in the middle of the grating [36].

Distributed Bragg reflector lasers have more advantages in comparison with external-grating, external cavity, C^3, and DBR, so there have been a lot of modifications and improvements in this device. Multiple-phase shift DFB, gain-coupled DFB, and multi-quantum well DFB structures are some samples of these improvements that have better characteristics in comparison with conventional DFB [37–39].

Although there have been many researches and investigations on DFB lasers, their optimization and characteristics investigation are on-going research subjects of recent years [40–50].

The main aim of this work will be modeling and analysis of a wavelength shifted distributed feedback (WDFB) laser. In this modeling, behavior and characteristics of the device, like threshold current, line width, power and spectrum of output wave, and laser stability in high power, will be investigated versus different physical and geometrical parameters such as the structure and size of the layers. The analysis method will be based on transfer matrix method (TMM).

2 Optical confinement factor

Time independent wave equation of electric field of an electromagnetic wave in a simple semiconductor laser is as follow [51]:

$$\nabla^2 E(x,y,z) + \varepsilon(x,y,z) k_0^2 E(x,y,z) = 0, \tag{1}$$

in which ε is dielectric constant, k_0 is defined by $k_0 = \frac{\omega}{c} = \frac{2\pi}{\lambda_0}$ and is wave number in free space.There is an identical equation for electromagnetic field component.

Transversal and lateral mode of the FB laser are obtained from the solution of pervious equation considering changes in directions of X and Y axis. An answer like Eq. (2) is supposed and applied to Eq. (1) that results in Eq. (3).

$$E_y(x,y,z) = \Phi(x)\Psi(y)(A\mathrm{e}^{\mathrm{i}\beta z} + B\mathrm{e}^{-\mathrm{i}\beta z}), \tag{2}$$

$$\frac{\mathrm{d}^2\Phi}{\mathrm{d}x^2} + \frac{\mathrm{d}^2\Psi}{\mathrm{d}y^2} + [\varepsilon(x,y)k_0^2 - \beta^2]\Phi(x)\Psi(y) = 0. \tag{3}$$

Generally, the effective index method (EIM) is applied to solve Eq. (3) [52]. In this method, the field transversal distribution is obtained from the solution of the following equation:

$$\frac{\mathrm{d}^2\Phi}{\mathrm{d}x^2} + [\varepsilon(x;y)k_0^2 - \beta_y^2(y)]\Phi(x) = 0, \tag{4}$$

in which β_y (y) is propagation constant for a fixed value of y, and $\varepsilon(x; y)$ is dielectric constant in each point of the laser. To solve Eq. (4), it is needed to consider boundary conditions including continuity of tangential component of the electric field and its derivatives at the interface between the layers. Lateral distribution of the optical field equation is obtained as

$$\frac{\mathrm{d}^2\Psi}{\mathrm{d}y^2} + [\beta_y^2(y) - \beta^2]\Psi(y) = 0, \tag{5}$$

for a specific structure, models of lateral and transversal modes are obtained from Eqs. (4) and (5), respectively. Effective refractive index is equal to

$$n_{\mathrm{eff}} = \mathrm{Re}(\beta/k_0), \tag{6}$$

the ratio of trapped light energy in the active layer of the laser to total light energy is called an optical confinement factor and is defined as follows:

$$\Gamma = \frac{\int\limits_{\text{active layer}} |E(x,y)|^2 \mathrm{d}x\mathrm{d}y}{\int_{\infty}^{\infty}\int_{\infty} |E(x,y)|^2 \mathrm{d}x\mathrm{d}y}, \tag{7}$$

transverse optical confinement factor is equal to

$$\Gamma_x = \frac{\left|\int\limits_{\text{active layer thickness}} \Phi(x)\right|^2 \mathrm{d}x}{\left|\int\limits_{\infty} \Phi(x)\right|^2 \mathrm{d}x}, \tag{8}$$

lateral optical confinement factor is equal to

$$\Gamma_y = \frac{\left|\int\limits_{\text{active layer width}} \Psi(y)\right|^2 \mathrm{d}y}{\left|\int\limits_{\infty} \Psi(y)\right|^2 \mathrm{d}y}, \tag{9}$$

the overall optical confinement factor is equal to

$$\Gamma = \Gamma_x\Gamma_y. \tag{10}$$

3 Rate equations

The rate equations that are the fundamental equations of semiconductor lasers, express the rate of changes in electrical carriers and also photons in time. From the solution of rate equations, the time-dependent function, frequency response, small signal, large signal and noise can be surveyed. Rate equations of electrical carrier and photons for multi-mode semiconductor laser can be written as follows [51]:

$$\frac{\mathrm{d}n}{\mathrm{d}t} = \frac{J}{qd} - (A + Bn + Cn^2)n - \sum_m G(n,\lambda_m,S_m)S_m, \tag{11}$$

$$\frac{\mathrm{d}S_m}{\mathrm{d}t} = [G(n,\lambda_m,S_m) - \gamma_m]S_m + R_{\mathrm{sp}m}, \tag{12}$$

in the above mentioned equations, J is input current density, q is the electron charge, d is the thickness of the active layer of the laser, A, B, and C are the non-radiative, self and Auger recombination rate, respectively. The last term in Eq. (11) is stimulated emission per time and per volume units for all modes. S_m is the density of photons in the mode of m, n is density of charge carriers, γ_m and G are defined as

$$G(n,\lambda_m,S_m) = v_{\mathrm{g}}g(n,\lambda_m,S_m), \tag{13}$$

$$\gamma_m = v_{\mathrm{g}}(\alpha_{\mathrm{in}} + 2\alpha_{\mathrm{th}}) \tag{14}$$

where v_{g}, $g(n,\lambda_m,S_m)$, α_{in}, α_{th} are group velocity, gain coefficient, internal dissipation factor and mode dissipation factor in threshold condition respectively. $R_{\mathrm{sp}m}$ in Eq. (12), spontaneous emission rate per unit volume, which is coupled with the m mode and its value is obtained from the following equation:

$$R_{\mathrm{sp}} = \beta_{\mathrm{sp}}Bn^2, \tag{15}$$

in which, β_{sp} is the spontaneous emission factor and its value is between 10^{-5} to 10^{-3}. In FB laser, charge carrier and photon densities are constant along the cavity, but in DFB laser their values depend upon z. Photon density in each point is proportional with light field intensity on that point, which means

$$S_m = C_0\left(|E_{\mathrm{f}}(z)|^2 + |E_{\mathrm{b}}(z)|^2\right). \tag{16}$$

C_0 is the proportional constant, which is determined by the rate equations.

In the steady-state, $\mathrm{d}S_m/\mathrm{d}t$ and $\mathrm{d}n/\mathrm{d}t$ are 0. At the threshold condition, the stimulated emission is negligible, so the threshold current density is obtained from the following equation, where S_m is placed by 0 in the carrier's rate equation:

$$J_{\mathrm{th}} = qd(A + Bn_{\mathrm{th}} + Cn_{\mathrm{th}}^2)n_{\mathrm{th}}. \tag{17}$$

n_{th} is the charge carriers' density in threshold condition, and is obtained from the following equation:

$$n_{\mathrm{th}} = \frac{g_{\mathrm{th}}}{a_{\mathrm{n}}} + n_{\mathrm{t}}, \tag{18}$$

where g_{th} is the threshold gain coefficient and is equal to

$$g_{\mathrm{th}} = \frac{\alpha_{\mathrm{in}} + 2\alpha_{\mathrm{th}}}{\Gamma}, \tag{19}$$

where Γ is the optical power confinement factor in the active region.

From the time-dependent coupled wave equation of DFB laser, its rate equations can also be obtained [53–56].

4 Spectral line width

Dispersion phenomena in optical fibers results in wider optical pulses and limits modulation speed. Therefore, the single-mode lasers with narrow line width are used in optical communication systems.

The line widths in different optical resources have different origins. There are some reasons that result in wider visible line in semiconductor lasers. Coincidental phase of spontaneous emission that are coupled to the excited modes of laser, gain to frequency dependency, variations and plunges in local charge carrier density and also interactions between photons and electrical changes are the main reasons [57,58].

Spectral width at half maximum optical power is measured as line width. The line width resulted from spontaneous emission effect in single mode semiconductor laser is mainly analyzed based on phase and amplitude of time-dependent classical electromagnetic wave based on following [59]:

$$\Delta\nu = \frac{R_{\mathrm{sp}}(1+\alpha_{\mathrm{H}}^2)}{2\pi I}, \tag{20}$$

in which R_{sp}, I and α_{H} are the rate of spontaneous emission, total number of photons in cavity, and line width enhancement factor, respectively. The latter is defined as [60]:

$$\alpha_{\mathrm{H}} = 2k_0 \frac{\frac{\mathrm{d}n_{\mathrm{r}}}{\mathrm{d}n}}{\frac{\mathrm{d}g}{\mathrm{d}n}}, \tag{21}$$

$\frac{\mathrm{d}n_{\mathrm{r}}}{\mathrm{d}n}$ and $\frac{\mathrm{d}g}{\mathrm{d}n}$ are change rates in refractive index and gain versus injected charge carrier density. The factor was first introduced by Henry [57] to justify experimental results. The acceptable value for in InGaAsP/InP is between 4.5 and 7 [61].

α_{H} depends on the charge carriers and photons densities and in the case of constant carrier density decreases by an increase in photons' energy. On the other hand, it remains constant at the peaks of gain curve in different values of carrier densities [62]. Moreover, α_{H} depends on temperature such that by a decrease in temperature, its value decreases. Up to this day, no direct way is introduced to measure α_{H}. But different methods, such as noise measurement [61] and line width measurement [63] are used to determine it. These methods cannot be evaluated in a certain manner.

Using Eq. (20), DFB laser line width is calculated as following [64]:

$$\Delta\nu = \frac{v_{\mathrm{g}}^2 n_{\mathrm{sp}} g_{\mathrm{th}} \alpha_{\mathrm{th}} h\nu (1+\alpha_{\mathrm{H}}^2)}{4\pi(P_1+P_2)}, \tag{22}$$

in which v_{g} is group velocity, n_{sp} is spontaneous emission factor, h, ν, P_1 and P_2 are Plank's constant, frequency, laser output power at left and right sides, respectively.

5 Output optical power of distributed feedback (DFB) laser

Output power of laser is proportional to the numbers of photons that are emitted from active region and exit from to end sides of the cavity in time unit. If the total numbers of photons in the laser is S_0, the output power of left and right sides can be obtained from following [65,66]:

$$P_1 = h\nu v_{\mathrm{g}}(1-R_1)\frac{|E_{\mathrm{b}}(0)|^2}{\left|\int_0^L E(z)\right|^2 \mathrm{d}z} S_0, \tag{23}$$

$$P_2 = h\nu v_{\mathrm{g}}(1-R_2)\frac{|E_{\mathrm{f}}(L)|^2}{\left|\int_0^L E(z)\right|^2 \mathrm{d}z} S_0, \tag{24}$$

where R_1 and R_2 are the reflection coefficient of the sides. The total number of photons at point is proportional to the square amplitude of sweep wave at that point. It can be obtained from the solutions of the rate equations and the coupled wave equations. The output power curve versus injected current is an important characteristic of the semiconductor lasers.

6 Spectrum of amplified spontaneous emission (ASE) in distributed feedback (DFB) laser

The spectrums of amplified spontaneous emission for the currents lower and higher than threshold current are important characteristics of DFB laser. Spontaneous emission spectrum of DFB laser can be obtained utilizing Green's function and TMM methods as follows [67]:

$$P_{\mathrm{ASE}} = \frac{hc}{\lambda}\frac{(1-r_2^2)}{y_{22}+r_1 y_{21}-r_2 y_{12}-r_1 r_2 y_{11}}\int_0^L n_{\mathrm{sp}}(z)g(z)|E(z)|^2 \mathrm{d}z. \tag{25}$$

In this equation, r_1, r_2, n_{sp}, y_{ij} are reflection coefficient of left and right side of the laser, inverse mass factor and matrix elements [68,69], respectively. $E(z)$ is the solution of coupled wave equation and P_{ASE} can be normalized to $\frac{hc}{\lambda}$.

To calculate, P_{ASE} in the threshold condition is replaced by g_{th} in Eq. (25), but in case of heir than threshold, it is calculated in term of charge carrier density from Ref. [70]. It should be noted that in latter condition its value depends upon z.

Utilizing ASE spectrum, it is possible to determine some parameters, such as frequencies of oscillation modes in lasers, frequency distance between successive modes, line width, the power difference between successive modes and changes in the wavelength of modes correspond to input current changes.

7 Side mode suppression ratio (SMSR)

Another important characteristic of semiconductor lasers is the ratio of main mode output power to the power of first side mode, which is called side mode suppression ratio (SMSR) and is defined as follows:

$$\mathrm{SMSR} = \frac{P_0}{P_s}, \tag{26}$$

where P_s is side mode power, P_0 is the power of main mode. SMSR is usually expressed in dB. Also, SMSR can be obtained by using the rate equations or ASE spectrum. An acceptable criterion for a single-mode laser is having a SMSR value more than 25 dB [51,70]. The SMSR value of the DFB laser is typically much higher than that of FP laser, and it increases by an increase in current. It should be mentioned that the spatial hole burning (SHB) effect far above the threshold current causes a reduction in SMSR value [71].

SMSR quantity is in direct proportion with the deference between the main and side modes. α_0 and α_1 are threshold gains of main and side modes, respectively, and $\Delta\alpha = \alpha_1 - \alpha_0$ is called gain margin. Gain margin can be considered as a criterion for single-mode laser evaluation. It is empirically known that in order to have a stable function, the single-mode laser should be more than 0.25 ($\Delta\alpha L \geqslant 0.25$) [71].

8 Laser structure

Ridge waveguide-quarter-wavelength shift distributed feedback (RW-QWS-DFB) laser has attracted more attention in comparison with other lasers due to its lower threshold current, higher power, and easer manufacturing process. In this section, the structure of RW-QWS-DFB at threshold and above threshold is analyzed based on the TMM method and its characteristics dependency to ridge width is investigated. A simple illustration of DFB laser with a ridge waveguide is shown in Fig. 1.

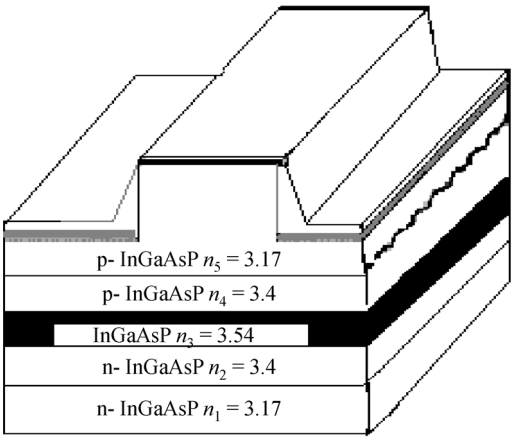

Fig. 1 Simple illustration of DFB 5-layered semiconductor laser

9 Simulation

Optical power confinement factor and coupling factor for RW-DFB structure is described in Section 2. This method can also be applied to RW-QWS-DFB structure. Figure 2 illustrates optical power confinement factor changes versus ridge width, w, for two different values of the active layer and waveguide thicknesses. As it shows, by increasing w, thelateral confinement factor coefficient increases; and for w = 5 μm, it tends to unity.

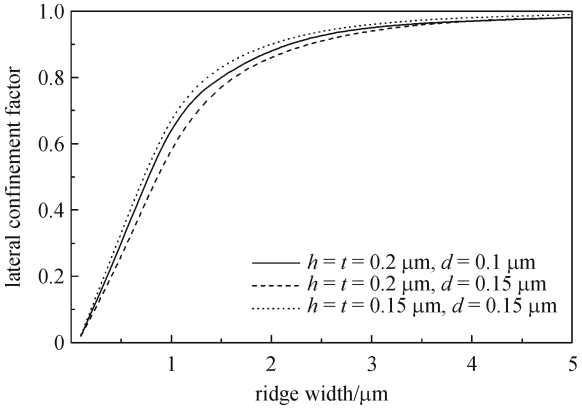

Fig. 2 Lateral confinement factor changes versus ridge width

Coupling coefficient variations versus ridge width is shown Fig. 3 for the same structures of Fig. 1. Coupling coefficient decreases with an increase in ridge width, such that for w = 5 μm the coupling coefficient is so close to a ridge less structure. The reason is that by decreasing the width of the ridge, the effect of side dielectric layers coated on the last layer on wave reflection increases. This happens in a condition that the amplitude of wave is damping in

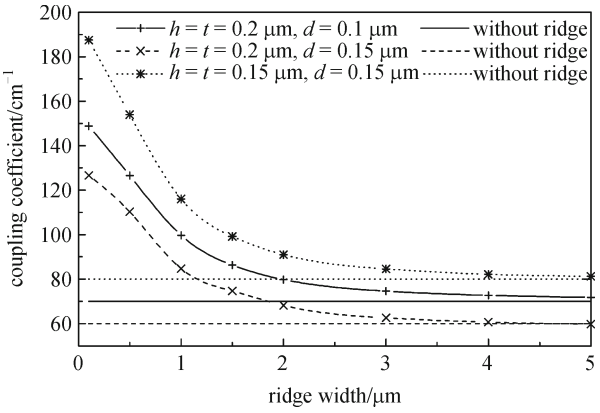

Fig. 3 Coupling coefficient changes versus ridge width in different thickness of active layers and waveguides

ridge area. Coupling coefficient of a ridge less structure is shown in the figure. It is observed that the coupling coefficient decreases by an increase in the thickness of the active layer and the waveguide.

With increasing w, the threshold current density in RW-QWS-DFB structure decreases, as shown in Fig. 4. It is obvious that the changes J_{th} for the values of $w > 2$ μm are negligible.

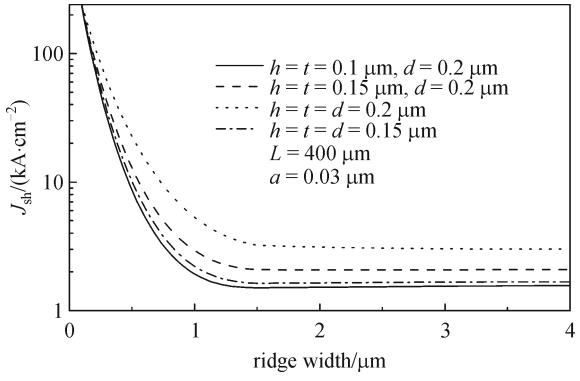

Fig. 4 Threshold current density changes versus ridge width in different thickness of active layers and waveguides

The threshold current changes in different width of ridge are depicted in Fig. 5. As it can be seen, it has its lowest current value in thickness between w = 1 and 2 μm.

Figures 4 and 5 are plotted for four different thicknesses of the active layer h, and the waveguide t. It can say that lower I_{th} and J_{th} values are due to higher coupling coefficient in structure with lower h and t.

10 Line width

Line width change of RW-QWS-DFB laser versus ridge width is shown in Fig. 6. It shows that with increasing w,

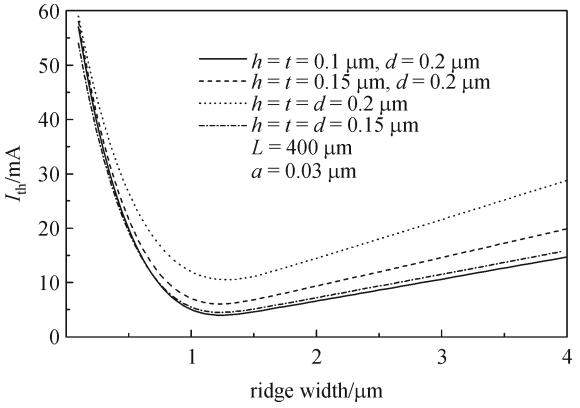

Fig. 5 Threshold current changes versus ridge width in different thickness of active layers and waveguides

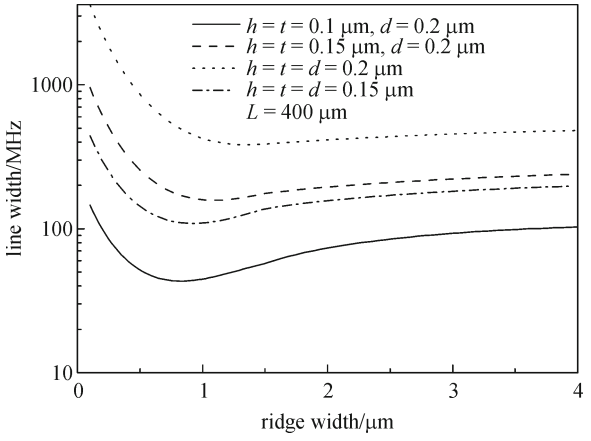

Fig. 6 Line width changes of RW-QWS-DFB laser versus different ridge widths

the line width decreases rapidly down to its minimum value that happens at $w \approx 1$ μm, and afterwards it start to increases slowly to offer the lowest increases. Moreover, the line width for higher t and h is more. As it can be seen that the line width is calculated for an output power of 1 mW.

The spectrum of amplified spontaneous emission of RW-QWS-DFB laser in threshold condition is shown in Fig. 7. This spectrum is analyzed for three different line widths w = 1, 3, 5 μm. As it can be seen that the structure with w = 1 μm has higher frequency gap in comparison with two other structures. Also, two other structures with w = 3, 5 μm have approximately equal frequency gaps.

Output power curve versus normalized current density (J/J_{th}) for the proposed RW QWS-DFB laser in two values of line widths can be seen in Fig. 8. Since coupling factor of w = 1 μm is higher, the output power and the slope of output power line versus J/J_{th} is lower in comparison with w = 3 μm.

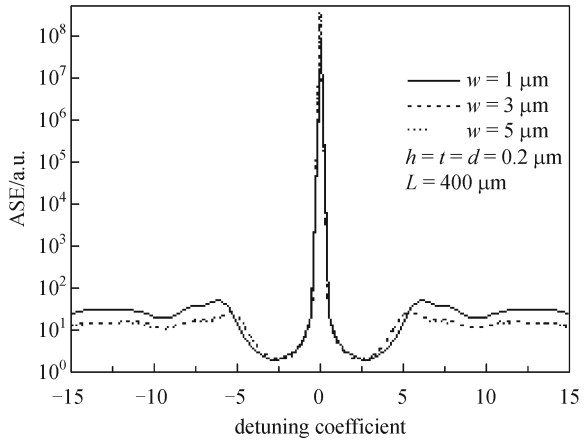

Fig. 7 Spectrum of ASE of RW-QWS-DFB laser in threshold condition for three different line widths w = 1, 3, 5 μm

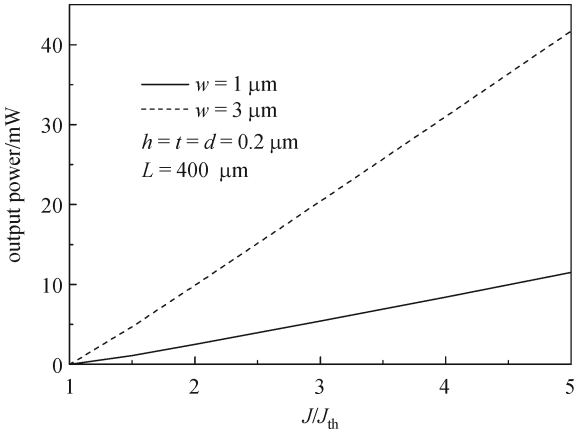

Fig. 8 Output power versus normalized current density for RW-QWS-DFB laser for two different value of w

Line width changes, $\Delta\nu$, of the proposed structure versus J/J_{th} is shown in Fig. 9 in w = 1 and 3 μm. As it is expected, by increasing current density, line width decreases. Due to lower output power in w = 1 μm, $\Delta\nu$ is more than its corresponding value in w = 3 μm.

Longitudinal distribution of photons and charge carrier density for w = 1 and 3 μm in above threshold condition is shown in Fig. 10. These figures show that photons distribution for w = 3 μm is more uniform than that for w = 1 μm, because it has a bigger valley in the center of photons distribution. Also the curves for charge carrier densities (Fig. 11) have the same trend while w = 1 μm shows bigger valley in center of the curve. These trends depict SHB effect in w = 1 μm structure. Moreover, the average increase of photons and carriers density is higher for w = 1 μm in comparison with w = 3 μm.

The average changes of the normalized threshold gain, αL, and the deviation from the Bragg normalized

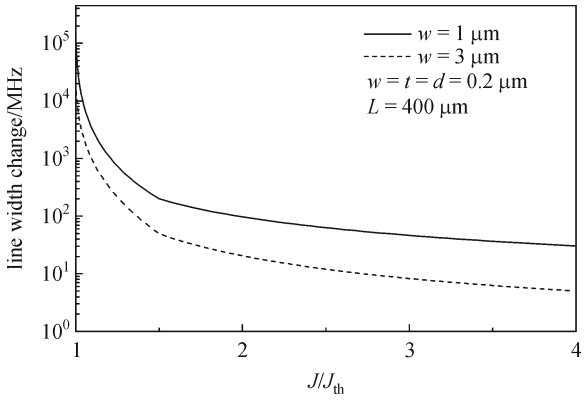

Fig. 9 Line width changes versus J/J_{th} for the proposed RW-QWS-DFB structure in w = 1 and 3 μm

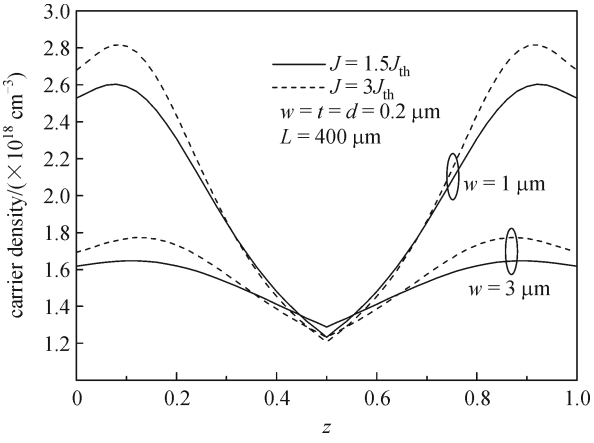

Fig. 10 Photons density distribution along the cavity of RW-QWS-DFB structure for w = 1 and 3 μm in above threshold condition

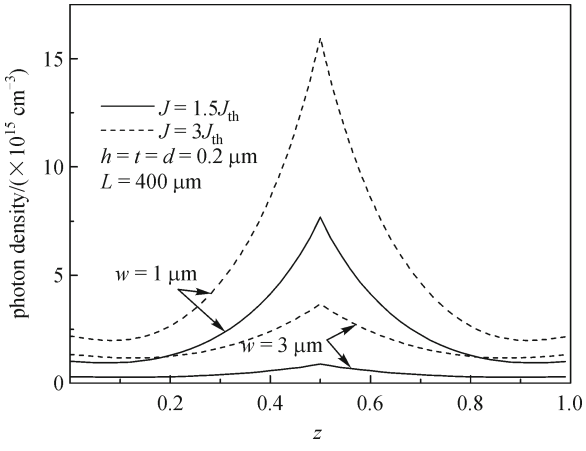

Fig. 11 Charge carrier density distribution of RW-QWS-DFB structure for w = 1 and 3 μm in above threshold condition

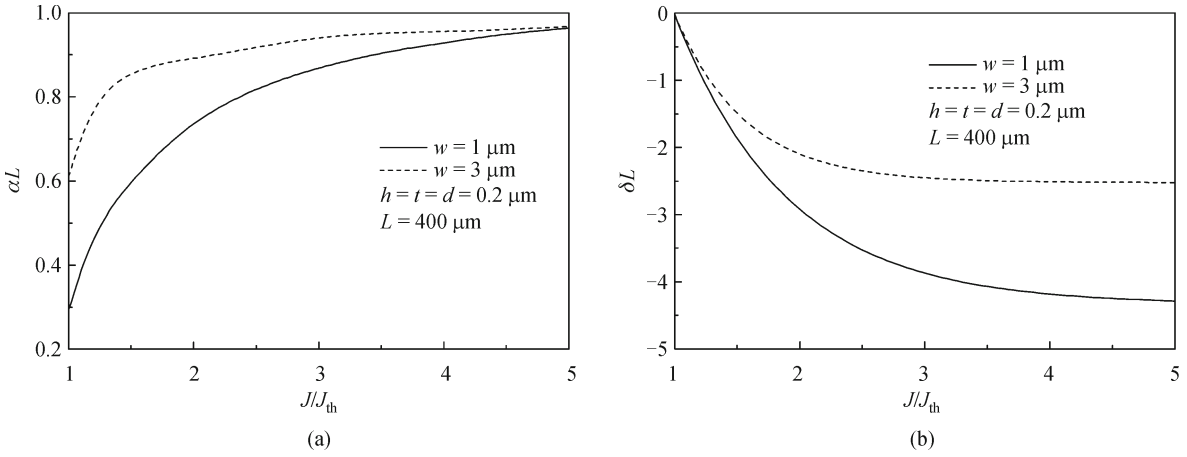

Fig. 12 (a) Average changes of the normalized threshold gain αL; (b) deviation from the Bragg normalized condition δL (J/J_{th} for two different ridge widths of w = 1 and 3 μm)

condition, δL, in terms of J/J_{th} are investigated in Figs. 12(a) and 12(b). As it can be seen, there are significant changes in these quantities versus input current. As it can be predicted form Fig. 4, the changes of αL and δL in w = 1 μm is more than that in w = 3 μm, because this two parameters' variations are due to changes in charge carrier density, which in turns depend on input current changes.

Figures 13(a) and 13(b) show laser output wave spectrum for two different ridge widths (1, 3 μm) in three different values of J/J_{th} = 1.02, 1.5 and 3. As these figures indicate that by increasing current, the power of the main mode and the side modes increase, but for w = 1 μm, the ratio of main mode power to side mode power decreases in high currents.

Also these figures indicate the changes of the main mode oscillation wavelengths in different input current density. Moreover, the main mode oscillation wavelength for w = 1 μm is slightly greater than its corresponding value for w = 3 μm with a difference of about 0.5 nm.

The output wave spectrum of RW-QWS-DFB laser in two different ridge widths for J/J_{th} = 3 are compared in Fig. 14. As it shows, for w = 1 μm, the side modes appear with more power in comparison with w = 3 μm.

Investigation of the SMSR parameter changes versus input current for two widths of w = 1 3 μm is shown in Fig. 15. The results verify the outcomes of Figs. 13(a) and 13 (b). As it can be seen, for w = 1 μm and $J/J_{th} > 1.8$, the SMSR parameter decreases with an increase in input current.

In this section, the uniformity parameter F, which dependences on the RW-QWS-DFB ridge width, is investigated. Figure 16 shows the F variation in terms of w. In this figure, the solid and fold (dashed) curved lines are corresponded to RW-QWS-DFB structure and horizontal straight lines show uniformity parameter in the QWS-DFB structure without ridge waveguide and with identical active layer thickness and waveguide.

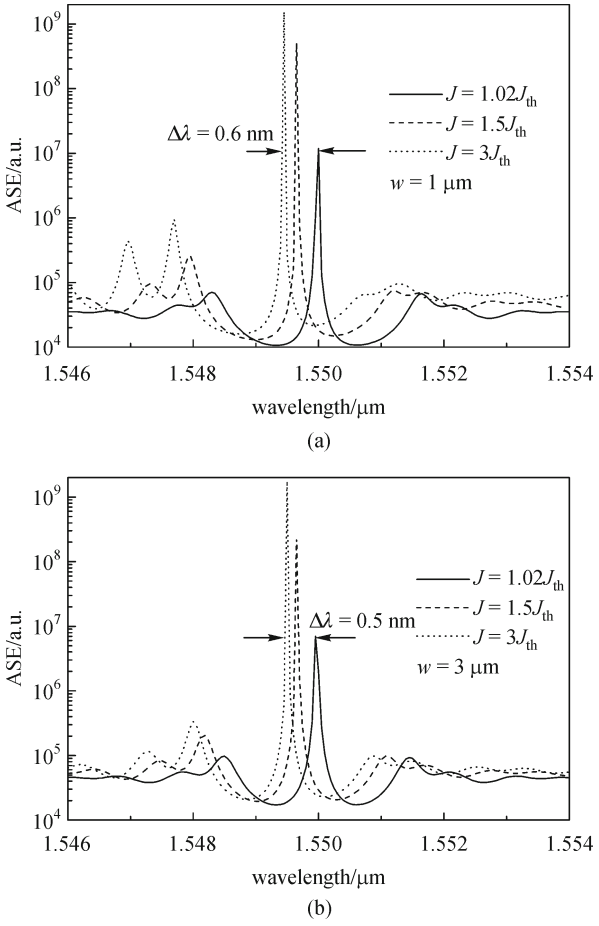

Fig. 13 Output wave spectrum for RW-QWS-DFB for J/J_{th} = 1.02, 1.5 and 3. (a) w = 1 μm; (b) w = 3 μm

As it can be seen, with increasing w, the uniformity parameter of RW-QWS-DFB structure decreases such that it tends to reach to its corresponding value in ridge-less

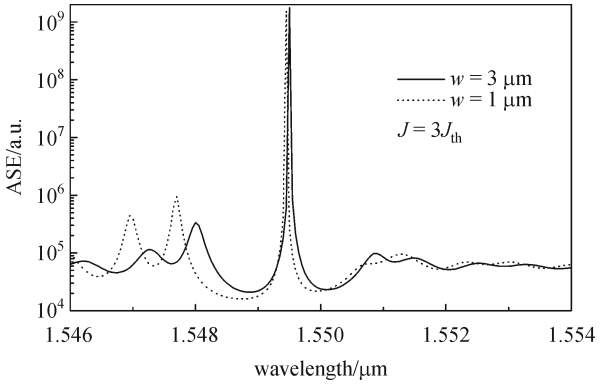

Fig. 14 Output wave spectrum of RW-QWS-DFB laser in two different ridge widths for $J/J_{th} = 3$

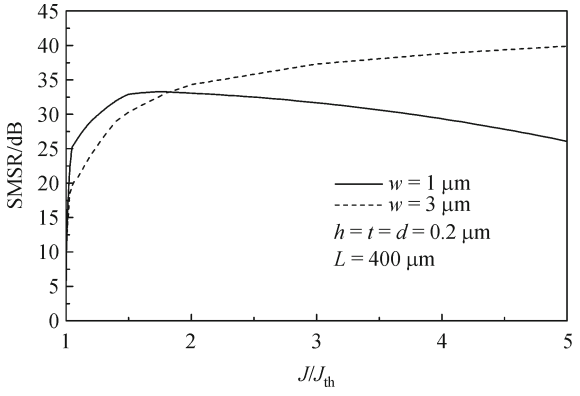

Fig. 15 SMSR changes versus input current for two widths of w = 1 and 3 μm in RW-QWS-DFB laser

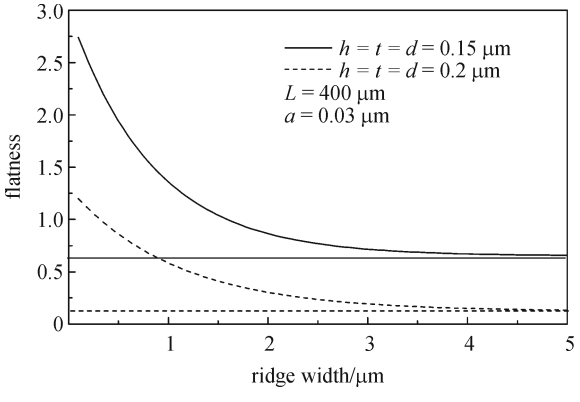

Fig. 16 Uniformity parameter dependence to RW-QWS-DFB ridge width. Curved lines represent RW-QWS-DFB structure and straight lines represent QWS-DFB structure

structure for higher values of w. Higher values of uniformity parameter at small widths are due to higher coupling coefficient that produces over coupling condition in the structure.

Optical field intensity distribution curve along the cavity of RW-QWS-DFB structure is shown in Fig. 17 that compares them for three values of w = 1, 3 and 5 μm. As this figure shows for w = 1 μm, strong coupling between the sweeping wave in the middle area of the laser causes an increase in optical field intensity, which produces over coupling condition in that parts. In this figure, optical field intensity distribution for a ridge-less structure is shown with open circle.

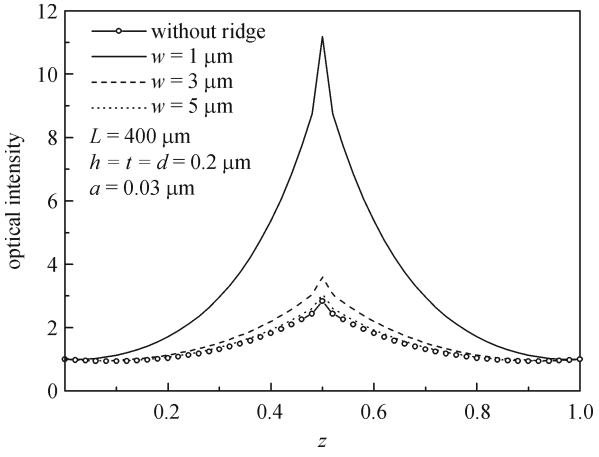

Fig. 17 Optical field intensity curve along cavity in RW-QWS-DFB structure in three different ridge widths

11 Conclusions

In this paper, the dependence of RW-QWS-DFB laser characteristics, such as coupling coefficient, threshold current and line width on ridge width, has been investigated for threshold and above threshold regions. It has been shown that an increase in ridge width (w) decreases the coupling coefficient, such that for w = 5 μm the coupling coefficient is very close to structure without ridge. In addition, study of threshold current versus ridge width have shown that for w = 1 μm to w = 3 μm threshold current has its minimum value and this current is also very less than its counterpart in structure without ridge. Moreover, study of RW-QWS-DFB laser line width versus ridge width has depicted that at first by increasing w, line width reduces sharply up to its minimum value at w about 1 μm and afterwards it increases slowly. The simulation result has shown that photons and charge carriers have more uniform distribution in w = 3 μm in comparison with that in w = 1 μm.

Acknowledgements This work was supported in part by Islamic Azad University.

References

1. Dumke W P. Interband transitions and maser action. Physical

Review, 1962, 127(5): 1559–1563
2. Hall R N, Fenner G E, Kingsley J D, Soltys T J, Carlson R O. Coherent light emission from GaAs junctions. Physical Review Letters, 1962, 9(9): 366–368
3. Nathan M I, Dumk W P, Burns G, Dill F H, Lasher G. Stimulated emission of radiation from GaAs p-n junctions. Applied Physics Letters, 1962, 1(3): 62–64
4. Quist T M, Rediker R H, Keyes R J, Krag W E, Lax B, Mcwhorter A L, Zeigler H J. Semiconductor maser of GaAs. Applied Physics Letters, 1962, 1(4): 91–92
5. Holonyak N, Bevacqua S F. Coherent (visible) light emission from $Ga(As_{1-x}P_x)$ junctions. Applied Physics Letters, 1962, 1(4): 82–84
6. Born M, Wolf E. Principle of Optics. 6th ed. Oxford: Pergamon Press, 1985, Section 7.6.2
7. Hayashi I, Panish M, Foy F. A low-threshold room-temperature injection laser. IEEE Journal of Quantum Electronics, 1969, 5(4): 211–212
8. Kressel H, Nelson H. Close confinement gallium arsenide p-n junction laser with reduced optical loss at room temperature. RCA Review, 1969, 30: 106–113
9. Hayashi I, Panish M B. GaAs-Ga_xAl_{1-x} As heterostructure injection lasers which exhibit low thresholds at room temperature. Journal of Applied Physics, 1970, 41(1): 150–163
10. Alferov Z I, Andreev V M, Korolkov V I, Portnoi E L, Tretyako D N. Injection properties of n-Al_xGa_{1-x} As p-GaAs heterojunctions. Soviet Physics Semiconductors, 1969, 2(7): 843–845
11. Hayashi I, Panish M B, Foy P W, Sumski S. Junction lasers which operate continuously at room temperature. Applied Physics Letters, 1970, 17(3): 109–111
12. Alferov Z I, Andreev V M, Garbuzov D Z, Zhilyaev Y V, Morozov E P, Portnoi E L, Triofim V G. Investigation of the influence of the AlAs-GaAs heterostructure parameters on the laser threshold current and the realization of continuous emission at room temperature. Soviet Physics Semiconductors, 1971, 4(9): 1573–1575
13. Ripper J E, Dyment J C, D'Asaro L A, Paoli T L. Stripe-geometry double heterostructure junction lasers: mode structure and CW operation above room temperature. Applied Physics Letters, 1971, 18(4): 155–157
14. Burnham R D, Scifres D R. Etched buried heterostructure GaAs/GaAlAs injection lasers. Applied Physics Letters, 1975, 27(9): 510–512
15. Kaminow I P, Stulz L W, Ko J S, Miller B I, Feldman R D, Dewinter J C, Pollack M A. Low threshold ridge waveguide laser at 1.55 μm. Electronics Letters, 1983, 19(21): 877–879
16. Lee T P, Burrus C A, Miller B I, Logan R A. Al_xGa_{1-x} As double-heterostructure rib-waveguide injection laser. IEEE Journal of Quantum Electronics, 1975, 11(7): 432–435
17. Hill D R. 140 Mbit/s optical fiber field demonstration systems. In: Sandbank C P, ed. Optical Fiber Communication Systems. Chichester: John Wiley & Sons, 1980
18. Zah C E, Pathk B, Favire F J, Pathak B, Bhat R, Caneau C, Lin P S D, Gozdz A S, Andreadakis N C, Koza M A, Lee T P. Monolithic integration of multiwavelength compressive-strained multiquantum-well distributed-feedback laser array with star coupler and optical amplifiers. Electronics Letters, 1992, 28(25): 2361–2362
19. Young M G, Koren U, Miller B I, Chien M, KochT L, Tennant D M, Feder K, Dreyer K, Raybon G. Six wavelength laser array with integrated amplifier and modulator. Electronics Letters, 1995, 31 (21): 1835–1836
20. Katoh Y, Kunii T, Matsui Y, Kamijoh T. Four-wavelength DBR laser array with waveguide couplers fabricated using selective MOVPE growth. Optical and Quantum Electronics, 1996, 28(5): 533–540
21. Ghafouri-Shiraz H, Lo B S K. Distributed feedback laser diodes. Chichester: John-Wiley & Sons, 1996, chapter 1
22. Lang R, Kobayashi K. External optical feedback effects on semiconductor injection laser properties. IEEE Journal of Quantum Electronics, 1980, 16(3): 347–355
23. MatthewsM R, CameronK H, WyattR, DevlinW J. Packaged frequency-stable tunable 20 kHz linewidth 1.5 μm InGaAsP external cavity laser. Electronics Letters, 1985, 21(3): 113–115
24. Tsang W T. The cleaved coupled cavity (C^3) laser. In: Semiconductors and semimetals. New York: Academic Press, 1985, 22(B), chapter 5
25. Coldren L A, Koch T L. Analysis and design of coupled-cavity lasers-Parts 1: threshold gain analysis and design guidelines. IEEE Journal of Quantum Electronics, 1984, 20(6): 659–670
26. Tsang W T, Olsson N A, Linke R A, Logan R A. 1.5 μm wavelength GaInAsP C^3 lasers: single frequency operation and wideband frequency tuning. Electronics Letters, 1983, 19(11): 415–417
27. Nakamura M, Yariv A, Yen H W, Somekh S, Garvin H L. Optically pumped GaAs surface laser with corrugation feedback. Applied Physics Letters, 1973, 22(10): 515–516
28. Kogelnik H, Shank C V. Coupled-wave theory of distributed feedback lasers. Journal of Applied Physics, 1972, 43(5): 2327–2335
29. Nakamura M, Yariv A, Yen H W, Garmire E, Somekh S, Garvin H L. Laser oscillation in epitaxial GaAs waveguides with corrugation feedback. Applied Physics Letters, 1973, 23(5): 224–225
30. Scifres D, Burnham R, Streifer W. A distributed feedback single heterojunction diode laser. IEEE Journal of Quantum Electronics, 1974, 10(9): 790–791
31. Casey H C, Somekh S, Ilegems M. Room-temperature operation of low-threshold separate-confinement heterostructure injection laser with distributed feedback. Applied Physics Letters, 1975, 27(3): 142–144
32. Utaka K, Akiba S, Sakai K, Matsushima Y. Room-temperature CW operation of distributed-feedback buried heterostructure InGaAsP-InP laser emitting at 1.57 μm. Electronics Letters, 1981, 17(25–26): 961–963
33. Uematsu Y, Okuda H, Kinoshita J. Room temperature CW operation of 1.3 μm distributed feedback GaInAsP/InP lasers. Electronics Letters, 1982, 18(20): 857–858
34. Streifer W, Burnham R, Scifres D R. Effect of external reflectors on longitudinal modes of distributed feedback lasers. IEEE Journal of Quantum Electronics, 1975, 11(4): 154–161
35. Zhou P, Lee G S. Chirped grating λ/4-shifted distributed feedback laser with uniform longitudinal field distribution. Electronics Letters, 1990, 26(20): 1660–1661
36. Utaka K, Akiba S, Sakai K, Matsushima Y. λ/4-shifted InGaAsP DFB laser by simultaneous holographic exposure of positive and negative photoresists. Electronics Letters, 1984, 20(24): 1008–1010

37. Agrawal G P, Geusic J E, Anthony P J. Distributed feedback lasers with multiple phase-shift regions. Applied Physics Letters, 1988, 53 (3): 178–179
38. Thijs P J A, Tiemeijer L F, Binsma J J M, Van D T. Progress in long-wavelength strained-layer InGaAs(P) quantum-well semiconductor lasers and amplifiers. IEEE Journal of Quantum Electronics, 1994, 30(2): 477–499
39. Morthier G, Vankwikelberge P, David K, Baets R. Improved performance of AR-coated DFB lasers for the introduction of gain coupling. IEEE Photonics Technology Letters, 1990, 2(3): 170–172
40. Alam M F, Karim M A, Islam S. Effects of structural parameters on the external optical feedback sensitivity in DFB semiconductor lasers. IEEE Journal of Quantum Electronics, 1997, 33(3): 424–433
41. Yu S F. Dynamic behavior of double-tapered-waveguide distributed feedback lasers. IEEE Journal of Quantum Electronics, 1997, 33(8): 1260–1267
42. Fessant T. Multisection distributed feedback lasers with a phase-adjustment region and a nonuniform coupling coefficient for high immunity against spatial hole burning. Optics Communications, 1998, 148(1–3): 171–179
43. Kinoshita J. Analysis of radiation mode effects on oscillating properties of DFB lasers. IEEE Journal of Quantum Electronics, 1999, 35(11): 1569–1583
44. Winick K A. Longitudinal mode competition in chirped grating distributed feedback lasers. IEEE Journal of Quantum Electronics, 1999, 35(10): 1402–1411
45. Peral E, Yariv A. Measurement and characterization of laser chirp of multiquantum-well distributed-feedback lasers. IEEE Photonics Technology Letters, 1999, 11(3): 307–309
46. Hsu A, Chuang S, Fang W, Adams L, Nykolak G, Tanbun-Ek T. A wavelength-tunable curved waveguide DFB laser with an integrated modulator. IEEE Journal of Quantum Electronics, 1999, 35(6): 961–969
47. Shams-Zadeh-Amiri A M, Li X, Huan W. Above-threshold analysis of second-order circular-grating DFB lasers. IEEE Journal of Quantum Electronics, 2000, 36(3): 259–267
48. Fernandes C F. Hole-burning corrections in the stationary analysis of DFB laser diodes. Materials Science and Engineering B, 2000, 74 (1–3): 75–79
49. Wang J Y, Cada M. Analysis and optimum design of distributed feedback lasers using coupled-power theory. IEEE Journal of Quantum Electronics, 2000, 36(1): 52–58
50. Morrison G B, Cassidy D T, Bruce D M. Facet phases and sub-threshold spectra of DFB lasers: spectral extraction, features, explanations and verification. IEEE Journal of Quantum Electronics, 2001, 37(6): 762–769
51. Agrawal G P, Dutta N K. Semiconductor Lasers. 2nd ed. New York: Van Nostrand Reinhold, 1993
52. Adams M J, Wyatt R. An Introduction to Optical Waveguide. London: John Wiley & Sons, 1981
53. Nakano Y, Luo Y, Tada K. Facet reflection independent, single longitudinal mode oscillation in a GaAlAs/GaAs distributed feedback laser equipped with a gain-coupling mechanism. Applied Physics Letters, 1989, 55(16): 1606–1608
54. Morthier G, Baets R. Modelling of distributed feedback lasers. In: Compound Semiconductor Device Modelling. London: Springer-Verlag, 1993, chapter 7, 119–148
55. Vankwikelberge P, Morthier G, Baets R. CLADISS-a longitudinal multimode model for the analysis of the static, dynamic, and stochastic behavior of diode lasers with distributed feedback. IEEE Journal of Quantum Electronics, 1990, 26(10): 1728–1741
56. Morthier G. An accurate rate-equation description for DFB lasers and some interesting solutions. IEEE Journal of Quantum Electronics, 1997, 33(2): 231–237
57. Henry C H. Theory of the linewidth of semiconductor lasers. IEEE Journal of Quantum Electronics, 1982, 18(2): 259–264
58. Pan X, Olesen H, Tromborg B. Spectral linewidth of DFB lasers including the effects of spatial holeburning and nonuniform current injection. IEEE Photonics Technology Letters, 1990, 2(5): 312–315
59. Henry C H. Theory of spontaneous emission noise in open resonators and its application to lasers and optical amplifiers. Journal of Lightwave Technology, 1986, 4(3): 288–297
60. Sugimura A, Patzak E, Meissner P. Homogenous linewidth and linewidth enhancement factor for a GaAs semiconductor laser. Journal of Physics D: Applied Physics, 1986, 19(1): 7–16
61. Kikuchi K, Okoshi T. Measurement of FM noise, AM noise, and field spectra of 1.3 μm InGaAsP DFB lasers and determination of the linewidth enhancement factor. IEEE Journal of Quantum Electronics, 1985, 21(11): 1814–1818
62. Vahala K, Chiu L C, Margalit S, Yariv A. On the linewidth enhancement factor α in semiconductor injection lasers. Applied Physics Letters, 1983, 42(8): 631–633
63. Fujise M. Spectral linewidth estimation of a 1.5 μm range InGaAsP/InP distributed feedback laser. IEEE Journal of Quantum Electronics, 1986, 22(3): 458–462
64. Kojima K, Kyuma K, Nakayama T. Analysis of spectral linewidth of distributed feedback laser diodes. Journal of Lightwave Technology, 1985, 3(5): 1048–1055
65. Tromborg B, Olesen H, Pan X, Saito S. Transmission line description of optical feedback and injection locking for Fabry-Perot and DFB lasers. IEEE Journal of Quantum Electronics, 1987, 23(11): 1875–1889
66. Makino T. Transfer-matrix formulation of spontaneous emission noise of DFB semiconductor lasers. Journal of Lightwave Technology, 1991, 9(1): 84–91
67. Makino T, Glinski J. Transfer matrix analysis of the amplified spontaneous emission of DFB semiconductor laser amplifiers. IEEE Journal of Quantum Electronics, 1988, 24(8): 1507–1518
68. Agrawal G P, Bobeck A. Modeling of distributed feedback semiconductor lasers with axially-varying parameters. IEEE Journal of Quantum Electronics, 1988, 24(12): 2407–2414
69. Shahshahani F, Ahmadi V. Analysis of relative intensity noise in tapered grating QWS-DFB laser diodes by using three rate equations model. Solid-State Electronics, 2008, 52(6): 857–862
70. Osinsky M, Polish M, Adams M J. Gain spectra of quarternary semiconductor. In: Proceedings of the IEEE I (Solid-State and Electron Devices). 1982, 129(6): 229–236
71. Rabinovich W S, Feldman B J. Spatial hole burning effects in distributed feedback lasers. IEEE Journal of Quantum Electronics, 1989, 25(1): 20–30

Abbas Ghadimi received the B.Sc. degree in electronics from Amir Kabir University of Technology, Tehran, Iran, and the M.Sc. degree in electronics from the University of Guilan, Iran, and the Ph.D. degree in electronics from Islamic Azad University (IAU), Sciences and Research Branch, Tehran, Iran. He joined IAU, Lahijan Branch, Iran, in 2002, where he is currently Assistant Professor of Electronics. His current fields of interest are modeling and analysis of photodetectors, all-optical devices based nanostructures and nano electronic devices.

Alireza Ahadpour Shal received the B.Sc. degree in electronics from Amir Kabir University of Technology, Tehran, Iran, and the M.Sc. degree in electronics from Khaje Nasir Toosi University of Technology, Tehran, Iran. He joined Islamic Azad University (IAU), Lahijan Branch, Iran, in 2006, where he is currently Lecturer and a full-time Member of Academic Staff at Electronic Group. His fields of interests are optical communication systems and optical networking.